Theoretical Study on the Molecular Mechanism for the Reaction of VO_2^+ with C_2H_4

L. Gracia,[†] J. R. Sambrano,[‡] V. S. Safont,*[,†] M. Calatayud,[†] A. Beltrán,[†] and J. Andrés[†]

Departament de Ciències Experimentals, Universitat Jaume I, Box 224, 12080 Castelló, Spain, and Departamento de Matemática, Universidade Estadual Paulista, Box 473, 17033-360 Bauru, Brazil

Received: October 21, 2002; In Final Form: February 26, 2003

The complex reaction between VO_2^+ ($^1A_1/^3A''$) and C_2H_4 ($^1A_g/^3A_1$) to yield VO^+ ($^1\Delta/^3\Sigma$) and CH_3CHO ($^1A'/^3A''$) has been studied by means of B3LYP/6-31G* and B3LYP/6-311G(2d,p) calculations. The structures of all reactants, products, intermediates, and transition structures of this reaction have been optimized and characterized at the fundamental singlet and first excited triplet electronic states. Crossing points are localized, and possible spin inversion processes are discussed by means of the intrinsic reaction coordinate approach. Relevant stationary points along the most favorable reaction pathways have been studied at the CCSD/6-311G(2d,p)//B3LYP/6-311G(2d,p) calculation level. The theoretical results allow the development of thermodynamic and kinetic arguments about the reaction pathways of the title process. In the singlet state, the first step is the barrierless obtention of a reactant complex associated with the formation of a V−C bond, while in the triplet state a three-membered ring addition complex with the V bonded to the two C atoms is obtained. Similar behavior is found in the exit channels: the product complexes can be formed from isolated products without barriers. The reactant and product complexes are the most stable stationary points in the singlet and triplet electronic states. From the singlet state reactant complex, two reaction pathways are posssible to reach the triplet state product complex. (i) A mechanism in which a hydrogen transfer process is the first and rate limiting step and the second step is an oxygen transfer between vanadium and carbon atoms with a concomitant change in the spin state. The crossing point between singlet and triplet spin states is not kinetically relevant because it takes place at a later stage occurring in the exit channel. (ii) A mechanism in which the first stage renders a four-membered ring between vanadyl cation and the ethylene fragment and an oxygen−carbon bond is formed; on going from this minimum to the second transition structure, associated with a carbon−vanadium bond breaking process, the crossing point between singlet and triplet spin states is reached. The final step is the hydrogen transfer between both carbon atoms to yield the product complex. In this case the spin change opens a lower barrier pathway. The transition structures with larger values of relative energies for both reactive channels of VO_2^+ ($^1A_1$) + C_2H_4 (^1A_g) → VO^+ ($^3\Sigma$) + CH_3CHO ($^1A'$) present similar energies, and the two reaction pathways can be considered as competitive.

1. Introduction

Wide technological applications of metal oxides justify the necessity to understand their physical and chemical properties.[1,2] Numerous studies on the chemical reactions of these systems in the gas phase have been carried out to clarify their catalytic activity as well as the mechanism and intermediates in many important processes.[3] The study of the gas-phase chemistry can provide information about their intrinsic chemical reactivity and can contribute to a better understanding of their behavior in the condensed phase. Due to the recognition of their key role in many reactive processes, chemical reactions between metal oxides and hydrocarbons have received special attention by different research groups.[4−6] While their chemical reactivity has been exploited for many years, a prerequisite for a more extensive understanding of catalytic reactions is to discover the details on an atomic scale. Therefore, the knowledge of the corresponding molecular mechanisms represents a research topic of great interest.

The behavior of metal oxides is strongly influenced by the presence of multiple low-lying electronic states in these species. Therefore, during the course of the chemical reaction, the system can access these energetically quasi-degenerate states and adapt to different bonding situations. Then, spin inversions can occur on going from reactants to products. In principle, the reaction rate can be limited by a transition structure (TS) or by the rate to cross between different electronic states. It seems quite difficult to speculate the detailed mechanism of such reactions which may involve complex isomerization and dissociation channels.[7−10] Reactions that involve a change in the spin state and thus occur on two or more potential energy surfaces (PESs) represent a field of growing interest in chemical physics and have received much attention in recent years.[11−18] In these cases, the standard theoretical description of chemical reactivity based on the idea of spin conservation along the reaction path must be abandoned.[19−22] This fact opens the possibility to a nonadiabatic behavior, in which the most favorable reaction pathway does not remain on a single PES as it evolves from rectants to products.

Many experimental and theoretical findings provide evidence for the importance of nonadiabatic processes, ranging from photodissociations,[23,24] reactions between metal cations and water,[25−27] and organic,[28−31] inorganic,[32−34] or organometallic[35−40] chemistry in which states of different multiplicities determine

* To whom correspondence should be addressed. E-mail: safont@exp.uji.es. Fax: 34 964 728066.
[†] Universitat Jaume I.
[‡] Universidade Estadual Paulista.

10.1021/jp0222696 CCC: $25.00
Published on Web 04/03/2003

the minimum energy reaction pathway. Shaik et al.[21,41] define these reactions in terms of two-state reactivity where two spin surfaces connect reactants and products.

Castleman et al. have studied, by means of ion beam mass spectrometry coupled with a laser vaporization source, the reactions of vanadium oxide clusters of different stoichiometries, $V_xO_y^+$, with various compounds such as C_2H_2, C_2H_6, C_2F_6, CH_3CF_3, CCl_4, and CH_2F_2.[42−48] Among them, the title reaction $VO_2^+ + C_2H_4$ may be of particular interest due to its apparent simplicity and the importance of reactant vanadyl cation VO_2^+. Schwarz et al. have selected Fourier transform mass spectrometry to study the gas-phase reaction, while calculations have been carried out to obtain electronic and thermochemical properties of the reactivity pattern.[49] This study points out that the oxidation of ethene by the vanadyl cation proceeds via a conceptually new mechanism which involves a coupled oxidation and hydrogen migration. Because the laboratory study of such type of reactions is not easy, theoretical studies may provide useful information about the nature of the chemical rearrangement. Therefore, we have carried out the present theoretical work in order to elucidate in detail the molecular mechanism of the oxidation reaction between VO_2^+ and C_2H_4 to yield VO^+ and CH_3CHO. This is a subtle calculation, since the spin mutiplicity of the metal oxide changes on going from the reactants to products. Two electronic states are involved: the reactant, VO_2^+ ($^1A_1$), has singlet spin multiplicity, and with the singlet ethylene the reactant system is an overall spin singlet state, while the product, VO^+ ($^3\Sigma$), has a triplet spin multiplicity as ground state.

The primary focus of the present study has been the understanding of the factors controlling the products outcome; reaction pathways having singlet and triplet electronic states have been explored, and the corresponding stationary points have been characterized. Finally, the points at which crossing can occur between the two spin states have been determined.

The organization of the article is as follows: the computing methods and model systems are described in section 2. In section 3, the results are reported and discussed; in subsection 3.1 an overview of the stationary points is presented; in subsection 3.2, we discuss the results of the population analysis; in subsection 3.3, we focus on the free energy profiles; and in subsection 3.4, the crossing points are described. The main conclusions that arise from the current research are finally summarized in section 4.

2. Computing Methods

All computations are carried out using the GAUSSIAN98 program package.[50] The calculations were performed at first approximation at the unrestricted or restricted B3LYP level,[51,52] using the 6-31G* basis set recently developed by Pople and co-workers.[53] This is a reasonable choice for a first-order approach to a theoretical exploration of these systems, as previous works have shown.[54−56] The computing methods based in the density functional theory require, in general, smaller basis sets than standard correlation methods. However, for obtaining reliable energetics in systems involving ion−molecule complexes such as the one herein studied, the use of larger basis sets with diffuse functions on the heavy atoms and polarization functions on all atoms is preferred.[49] Then, the relevant structures have been reoptimized by using the standard all electron 6-311G(2d,p) and 6-311+G(2d,p) basis sets implemented in GAUSSIAN98. We have found that the second basis set does not properly describe the transition structures associated with hydrogen transfers, so that the results obtained by using the 6-311G(2d,p) basis set are used for the discussion. A comparison is offered between B3LYP/6-31G* and B3LYP/6-311G(2d,p) results. Finally, single-point CCSD/6-311G(2d,p)//B3LYP/6-311G(2d,p)[57] calculations are performed at selected structures.

The computed stationary points have been characterized as minima or TSs by diagonalizing the Hessian matrix and analyzing the vibrational normal modes. In this way, the stationary points can be classified as minima if no imaginary frequencies are shown or as TSs if only one imaginary frequency is obtained. The particular nature of TSs has been determined by analyzing the motion described by the eigenvector associated with the imaginary frequency transition vector (TV).[58] Thus, harmonic vibrational frequencies, zero-point and thermal energy corrections, and force constants were calculated. The standard temperature (298.15 K) and pressure (1 atm) were used to obtain Gibbs free energies at the B3LYP/6-31G* and B3LYP/6-311G(2d,p) levels. Furthermore, the intrinsic reaction coordinate (IRC) method[59,60] has been used to describe minimum energy paths from TSs to the corresponding minima along the imaginary mode of vibration using the algorithm developed by González and Schlegel[61] in the mass-weighted internal coordinate system.

To locate the crossings between states of different spin multiplicities, the procedure used by Yoshizawa et al.[29] has been selected. Starting from the TS closest to the crossing seams, the IRC path was traced down to the corresponding minimum. Thereafter, each optimized point along the IRC path was submitted to a single point energy calculation with the other electronic state. In this way, we obtain the crossing points (CPs) as the structures that have identical geometries and energies in the singlet and triplet states.

The PES of the system, that consists of nine atoms ($VO_2^+ + C_2H_4$), is a function of internal degree of freedom of dimension 21. The crossing seam between the two PESs is therefore a hyperline of dimension 20, and it is difficult to perform a detailed inspection of the crossing seam. Therefore, as mentioned above, we have carried out single-point energy calculations (in the triplet spin state) as a function of the structural change along the IRC of the singlet state, and vice versa. It must be noted that what we obtain are the CPs along the IRC paths: other CPs can be found in other regions of the multidimensional PESs. The set of CPs we obtain in this way can be considered as estimates of the minimal energy crossing points (MECPs) between singlet and triplet hypersurfaces. The true MECPs would be stationary points if the gradient was defined in an appropriate way. Its obtention, described for instance in ref 62, is out of the scope of the present work. However, as the intermediates and TSs describe the molecular mechanism from reactants to products and can be connected to each other following the IRCs paths, we feel that the CPs we found have mechanistic significance and will allow us to discuss the molecular mechanism. Each IRC was constructed from a total of 65 or 154 steps (B3LYP/6-31G* level) and of 75 or 143 steps (B3LYP/6-311G(2d,p) level) to an accuracy of 0.1 amu$^{1/2}$·bohr of *s*, in which *s* is the length of the IRC.

The natural population analysis has been made by using the natural bond orbital (NBO)[63,64] option as implemented in GAUSSIAN98.

3. Results and Discussion

3.1. Overview of the Stationary Points. The geometries of the stationary points at both singlet and triplet electronic states are depicted in Figures 1 and 2, respectively. We use the prefixes "s" and "t" to denote the structures in the singlet and triplet electronic states, respectively.

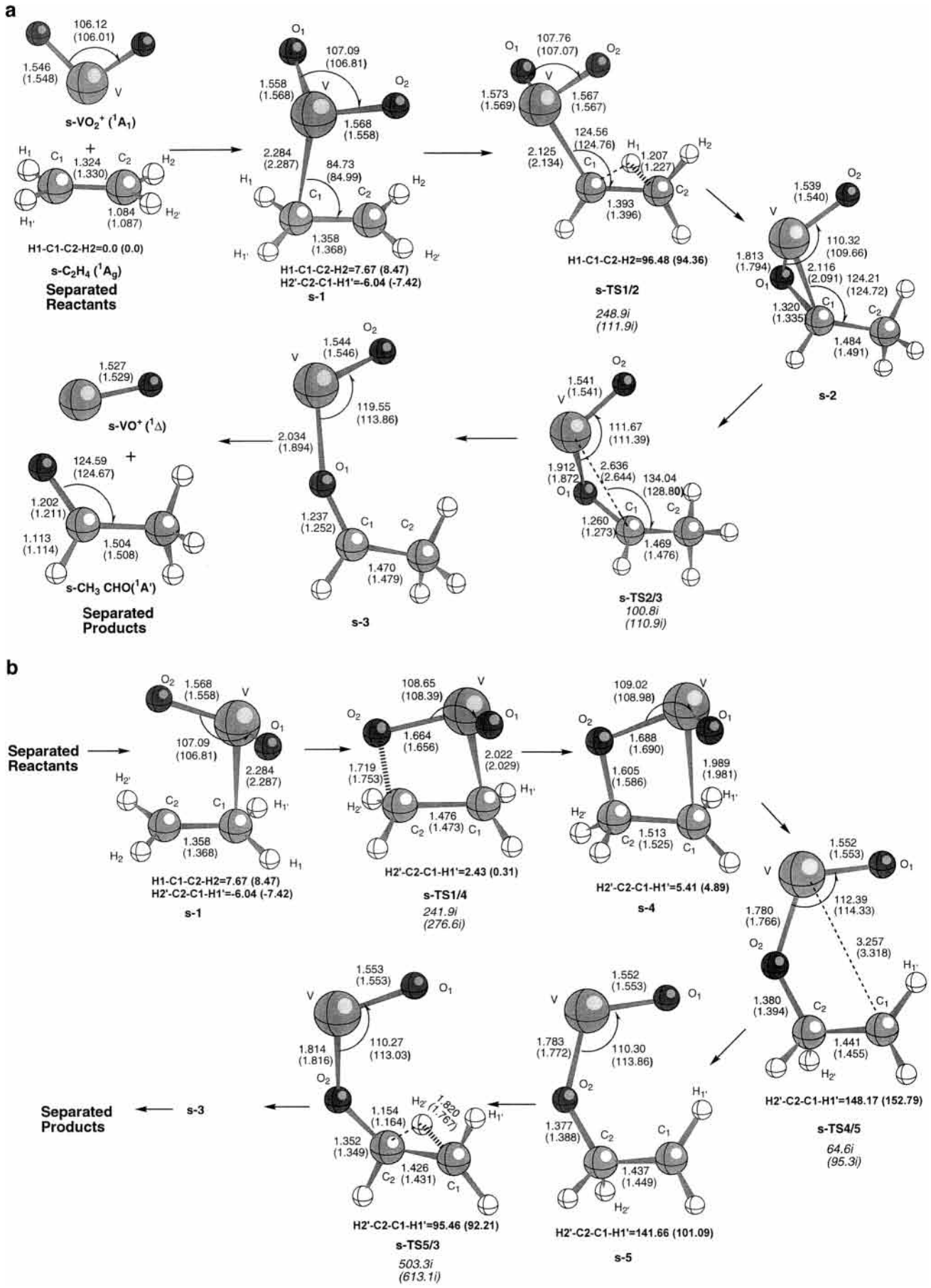

Figure 1. Structures (distances in Å and angles in deg) of the stationary points found in the first singlet electronic state at the B3LYP/6-311G-(2d,p) level and (in parentheses) at the B3LYP/6-31G* level. For TSs, the imaginary vibrational frequencies (cm^{-1}) are shown in italics. (a) First pathway. (b) Second pathway.

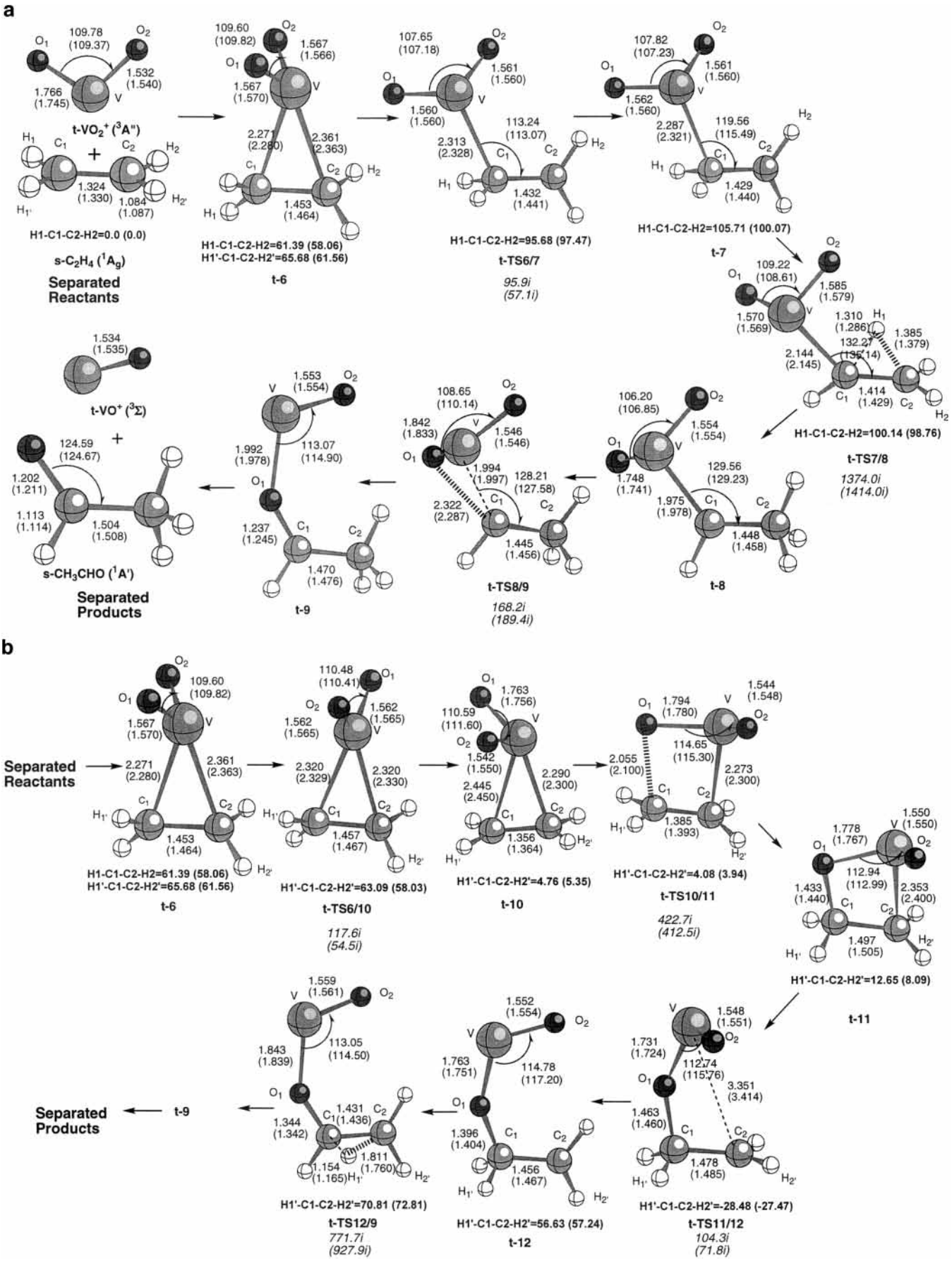

Figure 2. Structures (distances in Å and angles in deg) of the stationary points found in the first triplet electronic state at the B3LYP/6-311G(2d,p) level and (in parentheses) at the B3LYP/6-31G* level. For TSs, the imaginary vibrational frequencies (cm^{-1}) are shown in italics. (a) First pathway. (b) Second pathway.

An analysis of Figures 1 and 2 points out that the reactivity patterns of the singlet and triplet spin states are similar. The first stage of the reaction in both electronic states corresponds to the approach of vanadyl cation VO_2^+ toward the etyhlene fragment, with formation of the corresponding complexes: s-1 and t-6 for the singlet and triplet electronic states, respectively.

The geometry of s-1 (see Figure 1a, which presents the first reaction pathway in the singlet electronic state) points out that the interaction between vanadyl and ethylene systems takes place between V and one of the C atoms, yielding the formation of a V−C bond along a barrierless process. The next step is associated with an intramolecular hydrogen transfer between C_1 and C_2 to yield the s-2 intermediate, via the transition structure s-TS1/2. The channel from s-2 to s-3 takes place along s-TS2/3, associated with the cleavage and formation of C_1-V and C_1-O_1 bonds, respectively. The final stationary structure, s-3, can be viewed as a product complex and can be connected with the separated products.

A similar reaction pathway can be traced on the triplet state (Figure 2a). In t-6, an interaction takes place between V and both C atoms, and a three-membered ring is formed without a barrier. Then, a subsequent step connects t-6 with t-7 through t-TS6/7, associated with the opening of the C_2-C_1-V bond angle. From t-7, a hydrogen transfer process, via t-TS7/8, gives t-8. Thereafter, the C_1-O_1 bond formation and C_1-V bond breaking processes take place, via t-TS8/9, to render t-9. The last species, t-9, can also be viewed as a product complex and can be connected with the separated products.

The second pathway (Figure 1b: note that s-1 is viewed from the other side than in Figure 1a) begins with formation of a metallaoxetane species (s-4, similar to the triplet species t-11; see Figure 2b) through s-TS1/4. Then, an opening process of the four-membered ring renders s-5, that can be connected through another intramolecular hydrogen transfer step, s-TS5/3, to the intermediate s-3. In the triplet state, this reaction pathway includes a previous step, via t-TS6/10, yielding t-10. The main difference between t-6 and t-10 is the value of the rotation angle around the C_1-C_2 bond: the $H_{1'}-C_1-C_2-H_{2'}$ dihedral angle is ∼65 and ∼5° in t-6 and in t-10, respectively. Hence, from a chemical point of view, the π overlap between the p atomic orbitals of carbon atoms, that was not possible for t-6, is recovered at t-10. Thereafter, t-TS10/11 renders the metallaoxetane species (t-11) which, through a ring opening process, gives t-12. The final hydrogen transfer step, via t-TS12/9, yields t-9.

As can be seen, the calculated geometric parameters are roughly independent of the basis set size: in the singlet state the maximum difference in the reported distance values is 0.061 Å (C_1-V distance in s-TS4/5) and the difference in the reported angles is less than 5.69° (O_1-V-O_2 angle in s-3). The same trend is found with respect to the dihedral angles, except in s-5, for which the ethylene moiety is described as more planar at B3LYP/6-311G(2d,p) than at B3LYP/6-31G*. In addition, we must point out the difference observed in the $V-O_1$ distance, which is found to be slightly larger at the B3LYP/6-311G(2d,p) level, thus describing a less strongly bonded complex between the VO^+ and the acetaldehyde moieties. In the triplet state the differences in distances (lower than 0.063 Å), angles (lower than 4.07°), and dihedrals (lower than 5.64°) are also very small.

An analysis of the fluctuation patterns, that is, the atomic vibrations corresponding to the imaginary frequency, at TSs for the first pathway (Figures 1a and 2a) renders that the displacement of the H_1 atom is the main contribution to the TV corresponding to s-TS1/2 (and t-TS7/8 at the triplet electronic state), as expected (data not shown: TV components are available from the authors on request). In fact, the H_1 motion dominates the fluctuation pattern, mainly in t-TS7/8, while in s-TS1/2 a small but significant motion of C_2 and O_1 can be sensed. Hence, s-TS1/2 cannot be described only as a hydrogen transfer TS: the H_1 motion is coupled with some heavy atoms motions: C_2 approaches C_1 while O_1 moves away from C_1. This fact justifies the low imaginary frequency value obtained in the singlet state (around 250i cm^{-1}), compared with the higher value obtained in the triplet state (around 1370i cm^{-1}). Also, we must point out the different values for the imaginary frequency found for s-TS1/2 depending on the basis set used. For the small basis set the heavy atom motions are more intense, and consequently the imaginary frequency is lower (around 112i cm^{-1}). At s-TS2/3 (and also at t-TS8/9), the displacement of the O_1 atom is coupled with the motion of the $CHCH_3$ and VO fragments; therefore, the bond angle $V-O_1-C_1$ controls the TVs and this fact explains the low values for the imaginary frequencies. A similar behavior is found at t-TS6/7, and the orientation of the CH_2CH_2 moiety with respect to the VO_2 fragment controls the corresponding TV.

In what refers to the second pathway (Figures 1b and 2b), s-TS1/4 and t-TS10/11 are associated with the C−O bond formation, as can be seen either from the TV components or from the fluctuation patterns. s-TS4/5 and t-TS11/12, related with the V−C bond breaking, are quite different from each other from a geometrical point of view: the position of the oxygen atom is not bonded to the ethylene moiety and the two hydrogen atoms linked to the terminal carbon atom have different orientations. These differences can also be found in the TV components: s-TS4/5 is associated with dihedral angles as well as with the $V-C_1$ distance, while t-TS11/12 is only associated with the $V-C_2$ distance. The fluctuation pattern also differs: for s-TS4/5 the rotational motion of the CH_2 (of the terminal C atom) dominates, even over the vanadium atom motion, while for t-TS11/12 the coupled motions of C_2, O_1, and V atoms are the most significative. The hydrogen transfer TSs, s-TS5/3 and t-TS12/9, are essentially associated with the H motion from one carbon atom to the other. Finally, t-TS6/10 is located in a very flat zone of the PES, and a very low value of the imaginary frequency is found, mainly associated with the dihedral angle of the vanadyl moiety with respect the π system of the ethylene fragment.

The results that were obtained using 6-31G* are roughly recovered if the larger 6-311G(2d,p) is used instead. Although the imaginary frequency values slightly vary depending on the basis set size (see Figures 1a to 2b), the qualitative description of the processes remains.

3.2. Natural Population Analysis. In Table 1 the results of the natural population analysis for the stationary points are reported. The larger basis set renders a distribution of charges softer than the one obtained by the use of the small basis set, the differences being in general less than 0.2 au. This is what one could expect, due to the larger number of polarization functions used in the 6-311G(2d,p) basis set, thus permitting a further relaxation of the charge separation.

An electronic charge transfer (0.22 au) takes place from the ethylene moiety to the vanadyl cation at s-1 (see Table 1A); the negative charge of C_1 (the carbon atom linked to V atom) increases to −0.56 au, while the negative charge of the other carbon atom, C_2, is reduced to −0.17 au. Therefore, the formation of the addition complex, s-1, is an electrophilic attack of the VO_2^+ fragment on the π system of the olefin. In the triplet state (see Table 1B) an electronic charge (0.36 au) is

TABLE 1. Natural Population Analysis for the Stationary Points:[a] (A) Singlet State and (B) Triplet State

(A) Singlet State

	V	O_1	O_2	C_1	C_2	H_1	H_2	$H_{1'}$	$H_{2'}$
s-VO_2^+	1.60	−0.30	−0.30						
s-C_2H_4				−0.36	−0.36	0.18	0.18	0.18	0.18
s-1	1.50	−0.35	−0.37	−0.56	−0.17	0.26	0.23	0.24	0.23
s-TS1/2	1.42	−0.40	−0.40	−0.24	−0.48	0.36	0.26	0.21	0.26
s-2	1.48	−0.57	−0.37	0.18	−0.65	0.26	0.24	0.18	0.24
s-TS2/3	1.44	−0.66	−0.46	0.44	−0.68	0.24	0.26	0.16	0.27
s-3	1.39	−0.70	−0.52	0.57	−0.70	0.24	0.27	0.17	0.27

	V	O_1	O_2	C_1	C_2	$H_{1'}$	$H_{2'}$	H_1	H_2
s-1	1.50	−0.35	−0.37	−0.56	−0.17	0.24	0.23	0.26	0.23
s-TS1/4	1.48	−0.31	−0.46	−0.61	−0.09	0.24	0.24	0.26	0.24
s-4	1.49	−0.30	−0.48	−0.60	−0.09	0.24	0.24	0.26	0.24
s-TS4/5	1.49	−0.52	−0.74	−0.06	−0.15	0.21	0.26	0.21	0.30
s-5	1.46	−0.51	−0.74	−0.06	−0.15	0.21	0.28	0.21	0.29
s-TS5/3	1.37	−0.51	−0.74	−0.03	−0.11	0.22	0.32	0.22	0.26

	V	O	O	C (C═O)	C (CH_3)	H (CH_3)	H
s-VO^+	1.42	−0.42					
s-CH_3CHO			−0.52	0.46	−0.67	0.21	0.09

(B) Triplet State

	V	O_1	O_2	C_1	C_2	H_1	H_2	$H_{1'}$	$H_{2'}$
t-VO_2^+	1.61	−0.32	−0.28						
t-6	1.44	−0.40	−0.40	−0.30	−0.35	0.27	0.23	0.25	0.26
t-TS6/7	1.48	−0.36	−0.37	−0.40	−0.31	0.25	0.23	0.22	0.25
t-7	1.47	−0.37	−0.37	−0.41	−0.28	0.24	0.23	0.23	0.25
t-TS7/8	1.42	−0.39	−0.45	−0.41	−0.37	0.38	0.27	0.28	0.27
t-8	1.38	−0.26	−0.30	−0.13	−0.70	0.24	0.28	0.19	0.30
t-TS8/9	1.39	−0.30	−0.36	−0.05	−0.69	0.25	0.31	0.19	0.27
t-9	1.44	−0.69	−0.55	0.56	−0.70	0.24	0.27	0.17	0.27

	V	O_1	O_2	C_1	C_2	$H_{1'}$	$H_{2'}$	H_1	H_2
t-6	1.44	−0.40	−0.40	−0.30	−0.35	0.25	0.26	0.27	0.23
t-TS6/10	1.46	−0.23	−0.29	−0.44	−0.45	0.21	0.27	0.26	0.21
t-10	1.49	−0.31	−0.35	−0.26	−0.52	0.24	0.24	0.23	0.24
t-TS10/11	1.56	−0.49	−0.39	−0.14	−0.51	0.24	0.25	0.25	0.24
t-11	1.56	−0.64	−0.41	−0.12	−0.30	0.22	0.23	0.26	0.20
t-TS11/12	1.57	−0.69	−0.43	−0.09	−0.14	0.21	0.18	0.21	0.18
t-12	1.49	−0.72	−0.46	−0.13	−0.10	0.26	0.20	0.26	0.20
t-TS12/9	1.43	−0.78	−0.54	−0.10	−0.02	0.33	0.21	0.26	0.22
t-VO^+	1.46		−0.46						

[a] The calculated charge (au) on the indicated atoms, for the corresponding stationary points, is reported at the B3LYP/6-311G(2d,p) level.

also transferred from the ethylene moiety to the vanadyl cation at t-6. However, in this case, the values of the negative charges for the two carbon atoms, C_1 and C_2, remain roughly unaffected, due to the formation of a three-membered ring, and the positive charge increases in the terminal hydrogen atoms. Along the next step in the triplet eletronic state, t-6 → t-TS6/7 → t-7, this ring is opened, and the net electronic charge transferred from the ethylene fragment to the VO_2^+ moiety decreases to 0.27 au, a value slightly larger than the one found at s-1 (0.22, see above).

In the next step on the singlet electronic state (Figure 1a), s-1 → s-TS1/2 → s-2, the negative charge on C_1 disappears (+0.18 au at s-2), while that at C_2 increases until −0.65 au, as does, to a lower extent, that on O_1 (−0.57 au). At s-TS1/2, the hydrogen atom being transferred, H_1, is positively charged (0.36 au), and thus this process can be considered as a proton transfer, with negative charge migration from C_1 to C_2. In the stage t-7 → t-TS7/8 → t-8 (Figure 2a), the negative charge transfer from C_1 to C_2 has still not taken place at t-TS7/8. At t-8 the negative charge is located mainly on the C_2 atom (−0.70 au), and the negative charge on the O_1 atom is reduced (to −0.26 au) with respect to t-TS7/8, but the negative charge on C_1 remains because the C_1-O_1 bond is still not formed. At t-TS7/8, the positive charge of the transferred H_1 is 0.38 au.

At s-TS2/3 and s-3, the negative charges on the oxygen atoms increase, as well as the positive charge on the C_1 atom. At s-3, the VO^+ fragment polarizes the C_1-O_1 bond of ethanal, mainly in what refers to the negative charge on O_1 (−0.70 au). These effects, even increased, can be sensed in the triplet state for the step t-8 → t-TS8/9 → t-9.

On going from s-1 to s-4, via s-TS1/4 (Figure 1b), the negative charges on O_2 slightly increase, from −0.37 to −0.48 au, while on C_2 they slightly decrease (from −0.17 to −0.09), due to the formation of the C_2-O_2 bond. In the triplet state, for the consecutive steps t-6 → t-TS6/10 → t-10 and t-10 → t-TS10/11 → t-11 (Figure 2b) the charge on O_1 varies from −0.40 to −0.31 first and then from −0.31 to −0.64; on C1 the charge changes from −0.30 to −0.26 and then to −0.12. Note that in this case the C_1-O_1 is the bond being formed along the second stage.

At s-TS4/5 a huge discrepancy between the results obtained at the B3LYP/6-31G* and B3LYP/6-311G(2d,p) levels is found. The positive charge on the V atom is found to be 2.24 au by

using the small basis set, being only 1.49 au with the large one. Also, a significative diference is found in the negative charge on C_1 (−0.06 and −0.79 au depending on the basis set). The results at the B3LYP/6-31G* level describe a situation in which the C_1 atom still retains its negative charge, and as the C−V bond is almost broken, the vanadium is positively overcharged. The calculations with the small basis set seem to have addressed a wrong state. According to the results obtained at B3LYP/6-311G(2d,p), on going from s-4 to s-TS4/5 the negative charge on C_1 is reduced to −0.06 au, and the two oxygens take the negative charge, as a consequence of the C−V bond breaking. In the triplet state at t-TS11/12 the discrepancy is very small.

For s-TS5/3 and t-TS12/9, a positive charge is found on the hydrogen atoms being transferred, $H_{2'}$ (0.32) and $H_{1'}$ (0.33 au), respectively. Finally, in the s-3 and t-9 product complexes, the electronic charge transfer from the ethanal moiety to the VO^+ fragment presents small values: 0.13 and 0.11 au, respectively.

3.3. Free Energy Profiles. The Gibbs free energy profiles of the singlet and triplet electronic states are presented in Figure 3.

Four combinations are possible for the reactants and products, depending on their particular electronic states. The most stable combination of reactants is formed by VO_2^+ ($^1A_1$) and C_2H_4 (^1A_g) both in their singlet fundamental states, thus belonging to the overall singlet PES. The two triplet state combinations, t-VO_2^+ ($^3A''$) + s-C_2H_4 (^1A_g) and s-VO_2^+ ($^1A_1$) + t-C_2H_4 ($^3A_1$), stand 35.6 and 60.3 kcal/mol above the singlet (36.9 and 76.8 kcal/mol at the B3LYP/6-31G* level). The highest energy PES at the reactant side corresponds to the combination t-VO_2^+ ($^3A''$) + t-C_2H_4 ($^3A_1$), 95.9 kcal/mol above (113.7 kcal/mol at the B3LYP/6-31G* level).

In Figure 3a the relative free energies of the stationary points of the first pathway, with respect to the reactants in its singlet electronic state, are presented. Starting from the separated reactants, an inverted energy profile is found for the first steps. The first reaction path connects the reactants in its singlet state with s-1**,** s-TS1/2, s-2, s-TS2/3, and s-3. A final step from the product complex leads to the isolated products. The second reaction path **(**Figure 3b**)** connects the reactants in its singlet state with s-1, s-TS1/4**,** s-4, s-TS4/5, s-5, s-TS5/3, and s-3, with the final climb up to the products. A comparison between the values of the relative energies of the highest TSs for both channels shows that s-TS4/5 and s-TS5/3 have larger values (16.4 and 15.7 kcal/mol, respectively) than s-TS1/2 (−6.9 kcal/mol). Therefore, the first pathway is energetically favorable.

The most stable combination of products is formed by t-VO^+ ($^3\Sigma$) + s-CH_3CHO ($^1A'$), that belongs to the overall first triplet PES. The singlet PES, whose products would correspond to s-VO^+ ($^1\Delta$) + s-CH_3CHO ($^1A'$), is ∼26 kcal/mol above, while the two other combinations have higher energy values. Then, it is obvious that, from the most stable reactants to the most stable products, at least one crossing must take place. We will focus only on the possible crossings between the first singlet and triplet states, once the reactive complex (s-1) is formed. Higher excited triplet PESs, as well as quintuplet PESs, were not considered. It must be noted that the products combination t-VO^+ ($^3\Sigma$) + t-CH_3CHO ($^3A''$), that can be assigned a global spin state of singlet, triplet, or quintuplet, is well above the singlet products and also that the highest energy product combination, s-VO^+ ($^1\Delta$) + t-CH_3CHO ($^3A''$), corresponds to another triplet state PES.

In Figure 3c and d the relative energy (to the reactants in its singlet electronic state) is plotted against the stationary points found in the triplet state. Again, an inverted energy profile is found at least for the first steps of both possible pathways. The first reaction channel, going from the triplet state reactants to the triplet state products through t-6, t-TS6/7, t-7, t-TS7/8, t-8, t-TS8/9, and t-9, is depicted in Figure 3c. This channel is energetically unfavored with respect the second pathway (Figure 3d), that goes from the triplet state reactants to the products through t-6, t-TS6/10, t-10, t-TS10/11, t-11, t-TS11/12, t-12, t-TS12/9, and t-9. This second pathway lies always under the triplet state reactants energy, and therefore, no activation barrier has to be surmounted.

As can be seen in Figure 3, the use of one or another of the basis sets herein employed does not produce significative changes in what refers to the relative energies, with the only exception being separated products.

3.4. Crossing Points. The products in triplet state, VO^+ ($^3\Sigma$) + CH_3CHO ($^1A'$), will be formed from the reactants in singlet state, VO_2^+ ($^1A_1$) + C_2H_4 (^1A_g). Therefore, at least a crossing and spin inversion process must take place in the reaction pathway. Due to the fact that the CPs are not stationary points on either of the individual spin surfaces, we use potential energies, ΔE, instead of Gibbs free energies, ΔG, to obtain the energetic profiles. Hence, single-point energy calculations in the triplet state on the geometries optimized for the intermediates and TSs in the singlet state have been carried out. This procedure is used as the starting point to localize the crossing seams between singlet and triplet PESs. Also, from the stationary points found in triplet state, single-point energy calculations in singlet state have been performed to localize other crossings between triplet and singlet PESs.

A comparative analysis of the energy profiles using ΔE (not shown, available from the authors on request) instead of ΔG shows that both energetic criteria render rather similar results with respect to the relative energies of stationary points, minima, and TSs. Therefore, the energy profiles based on ΔE values are used to discuss the role of the CPs in the corresponding reaction pathways.

Four CPs are expected to occur according to the results of the analysis described above: between s-2 and s-TS2/3 (CP1); between s-4 and s-TS4/5 (CP2); between t-TS8/9 and t-9 (CP3); and between t-TS10/11 and t-11 (CP4). In Figure 4, the IRC paths calculated at the B3LYP/6-311G(2d,p) level from s-TS2/3 to s-2 and from s-TS4/5 to s-4, respectively, are shown as solid lines. Energy is plotted as a function of the IRC value scaled from 0 (the TS) to −1 (the corresponding minimum that precedes the TS in the reaction pathway, hence the negative sign). The dotted lines are the single-point energy values on the geometries of each optimized point along the IRC path, in triplet electronic state. The figures point out the crossing seams where the values of energy for both electronic states become equal for a determined geometry along the IRC path.

In Figure 4a it is shown that the energies of the singlet and triplet states coincide for a scaled IRC value of $s = -0.84$ (−0.73 at the B3LYP/6-31G* level, data not shown). The structure of this crossing point (CP1) is depicted in Figure 5. This point is geometrically closer to s-2 than to s-TS2/3: the V−C_1 distance is 2.168 Å. This distance is 2.116 Å in s-2 and 2.636 Å in s-TS2/3. Also, the O_1−C_1 distance in CP1 is 1.311 Å, compared to 1.320 Å in s-2 and 1.260 Å in s-TS2/3. Accordingly, the energy of CP1 is ∼0.3 kcal/mol over the s-2 energy, while the energy difference between s-TS2/3 and s-2 is ∼4.4 kcal/mol, and hence CP1 is also energetically closer to s-2 than to s-TS2/3.

The existence of CP1 opens the possibility for an intersystem crossing to take place. It is conceivable that a mechanistic path,

a

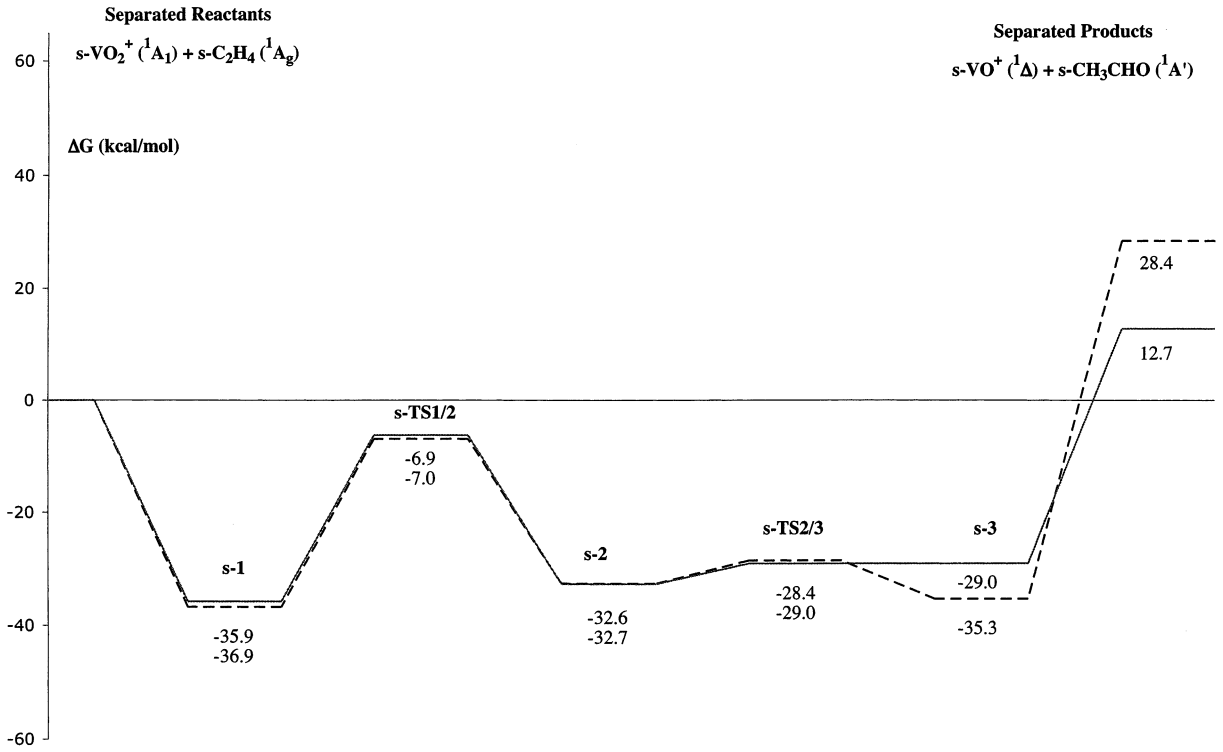
Separated Reactants
s-VO2+ (1A1) + s-C2H4 (1Ag)
Separated Products
s-VO+ (1Δ) + s-CH3CHO (1A')
ΔG (kcal/mol)
60
40
20
0
-20
-40
-60
28.4
12.7
s-TS1/2
-6.9
-7.0
s-1
-35.9
-36.9
s-2
-32.6
-32.7
s-TS2/3
-28.4
-29.0
s-3
-29.0
-35.3

b

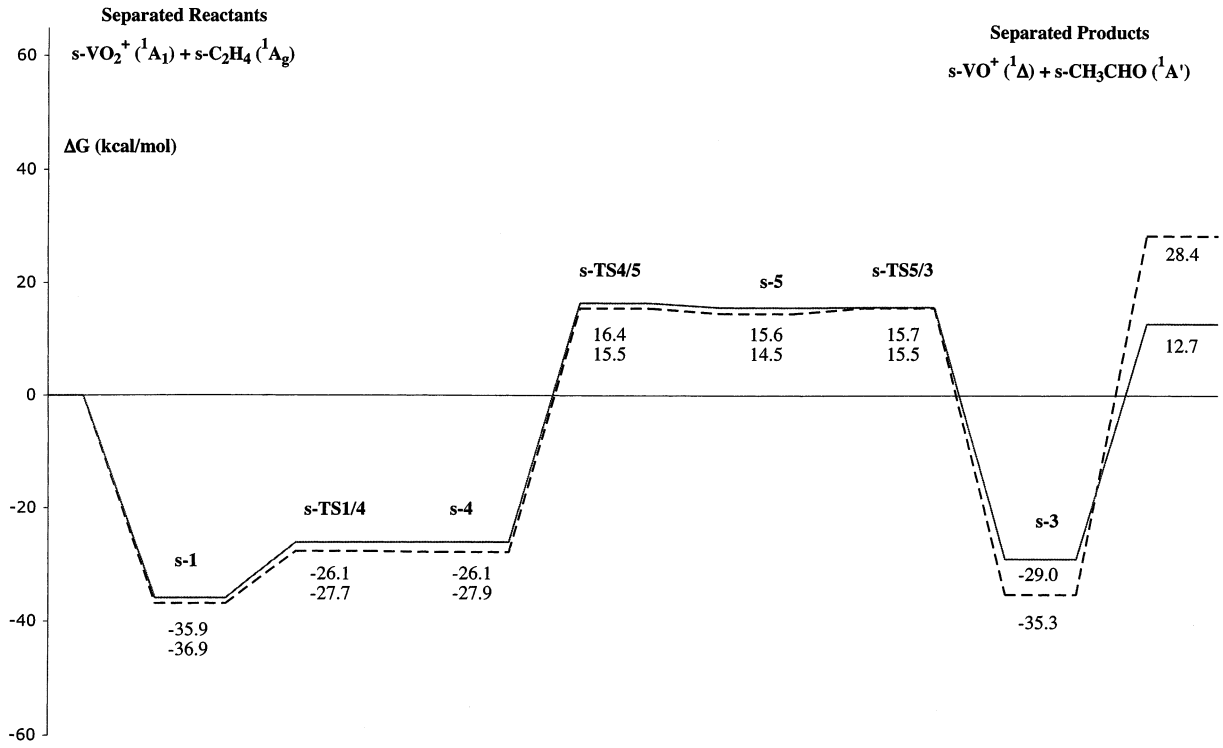
Separated Reactants
s-VO2+ (1A1) + s-C2H4 (1Ag)
Separated Products
s-VO+ (1Δ) + s-CH3CHO (1A')
ΔG (kcal/mol)
60
40
20
0
-20
-40
-60
28.4
12.7
s-TS4/5
16.4
15.5
s-5
15.6
14.5
s-TS5/3
15.7
15.5
s-TS1/4
-26.1
-27.7
s-4
-26.1
-27.9
s-1
-35.9
-36.9
s-3
-29.0
-35.3

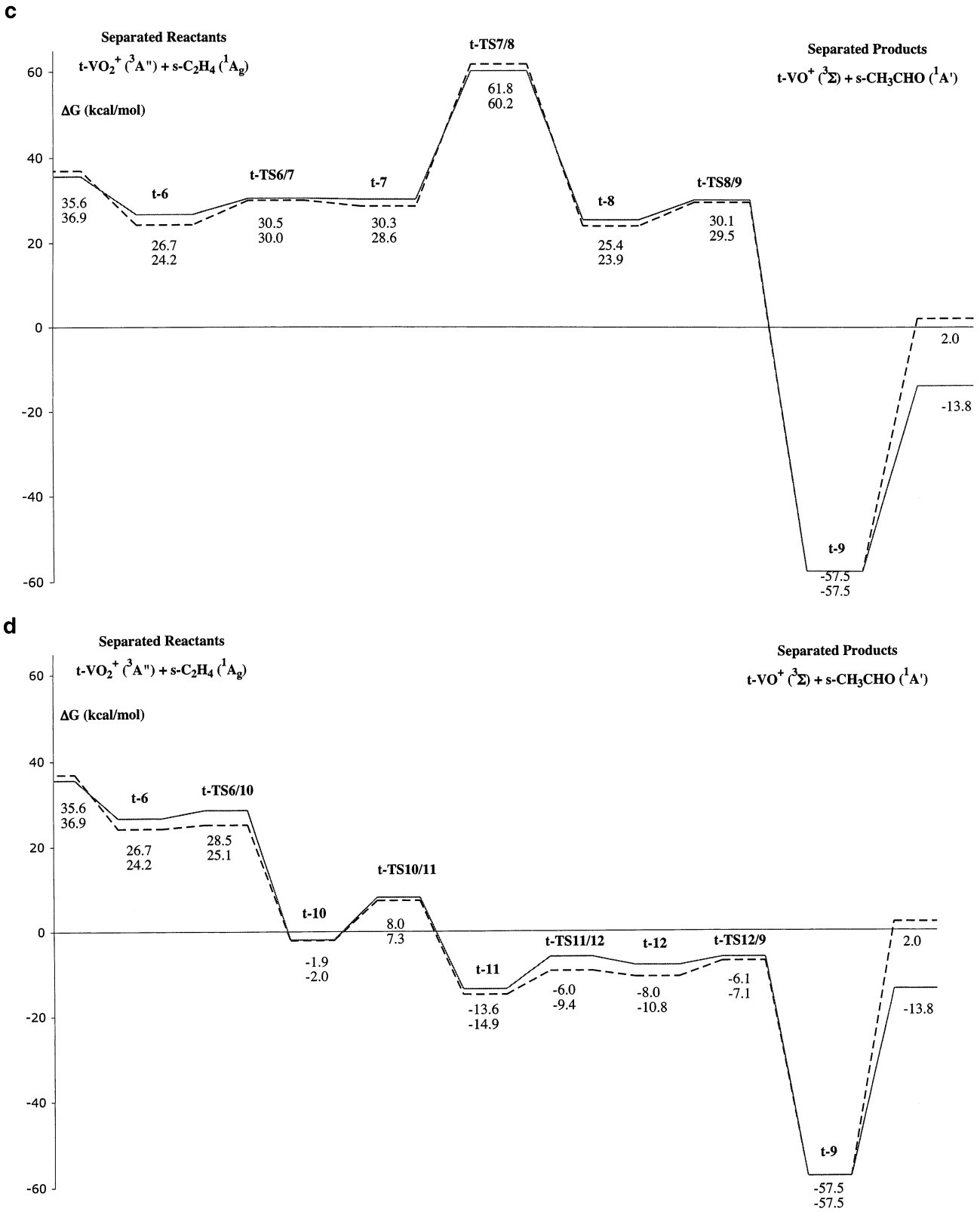

Figure 3. Gibbs free energy profiles at 298.15 K, relative to the reactants in the singlet state. (a and b) First singlet and (c and d) first triplet electronic states at the B3LYP/6-311G(2d,p) (solid lines) and B3LYP/6-31G* (dashed lines) levels. ΔG values (kcal/mol) are indicated. The total Gibbs free energy values of the singlet electronic state for the separated reactants are −1172.782 553 hartrees at the B3LYP/6-311G(2d,p) level and −1172.659 430 hartrees at the B3LYP/6-31G* level.

starting from the reactants in the singlet state, goes through s-1, s-TS1/2, and s-2. Then, before reaching s-TS2/3, CP1 is found, and a downhill path can be taken on the triplet state PES.

A full optimization has been carried out from the CP1 structure in triplet electronic state to find the corresponding stationary point. This optimization ends up at t-9, and therefore this minimum is directly reached from CP1. This can be geometrically justified: the C_1-V distance (the main variable controlling the steps from t-8 to t-9) is 2.168 Å in CP1. This value is larger than 1.975 Å (the value found at t-8) and also

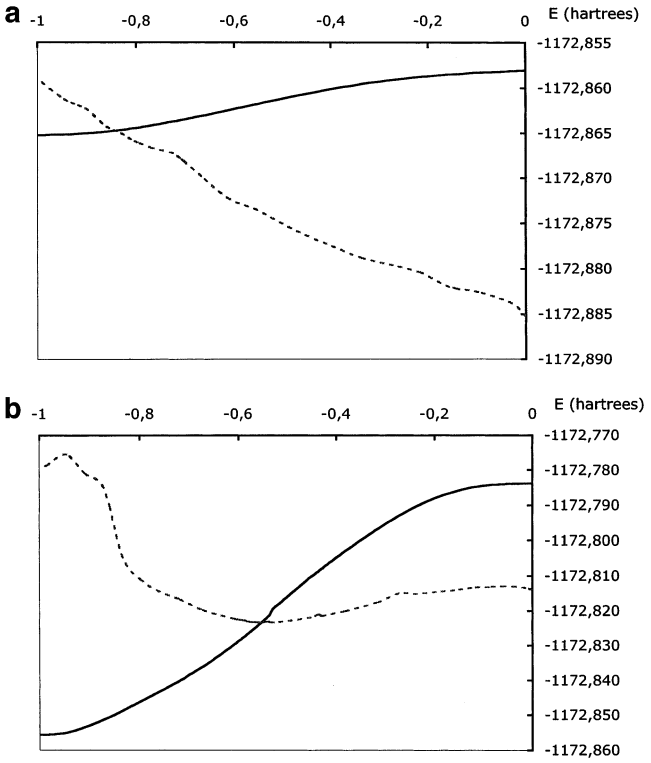

Figure 4. Potential energy (E, hartrees) along the IRC (amu$^{1/2}$·bohr, scaled from 0 to −1). (a) IRC path from s-TS2/3 (point at s equal to zero) to s-2 (s equal to −1), solid line. Dotted line: single-point energy values in the triplet electronic state. (b) IRC path from s-TS4/5 ($s = 0$) to s-4 ($s = -1$), solid line. Dotted line: single-point energy values in the triplet electronic state. B3LYP/6-311G(2d,p) results.

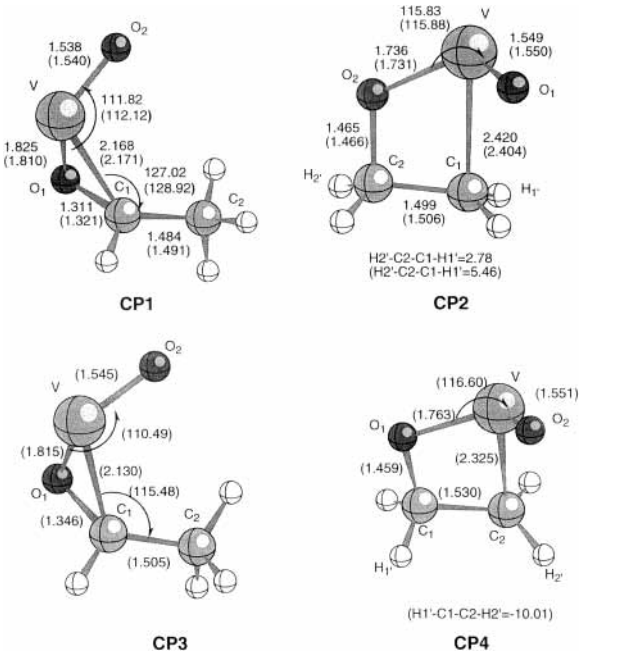

Figure 5. Structure of the crossing points found (bond distances in Å and angles in deg at the B3LYP/6-311G(2d,p) level and (in parentheses) the B3LYP/6-31G* level). (a) CP1, from s-TS2/3 to s-2. (b) CP2, from s-TS4/5 to s-4. (c) CP3, from t-TS8/9 to t-9. (d) CP4, from t-TS10/11 to t-11.

than 1.994 Å (the value found at t-TS8/9). Hence, from a geometric viewpoint, when the triplet surface is reached at CP1, the stationary points t-8 and t-TS8/9 are left behind, and a direct pathway is opened to t-9. It must be noted that CP1 is not kinetically relevant because the rate-limiting step of the resulting pathway (the passage over s-TS1/2) is located in a previuos stage, and the spin inversion is not regarded as a rate-limiting factor but rather as a later step occurring in the exit channel.

In Figure 4b, it is shown that, for a scaled IRC value of $s = -0.55$ (−0.57 at the B3LYP/6-31G* level, data not shown), the singlet and triplet states present similar energy. The structure of the corresponding crossing point (CP2) is shown in Figure 5. CP2 is similar to s-4: the V−C_1 distance is 2.420 Å in CP2, this value being 1.989 Å in s-4 and 3.257 Å in s-TS4/5. However, the O_2−C_2 bond distance is 1.465 Å in CP2, and this value is closer to 1.380 Å (the value found in s-TS4/5) than to 1.605 (the value at s-4). On the other hand, the energy of CP2 is 20.6 kcal/mol above that of s-4, while the energy difference between s-4 and s-TS4/5 is 45.1 kcal/mol. Therefore, CP2 is energetically closer to s-4 than to s-TS4/5.

CP2 opens the possibility for another intersystem crossing process to take place. The path would now start from the reactants in the singlet state, going through s-1, s-TS1/4, and s-4. Then, before reaching s-TS4/5, CP2 is found, and the path can be continued on the triplet state PES. Again, a full optimization has been carried out from the CP2 structure in triplet electronic state. This optimization ends up in t-11. The conclusion, hence, is that, from CP2, t-11 is reached. From this point onward, the path would continue on the triplet surface, through t-TS11/12, t-12, and t-TS12/9, to reach t-9 and finally the products. It must be noted that, in this case, CP2 is reached before the rate-limiting step of the resulting pathway, and therefore the spin inversion can be kinetically relevant, because it takes place in the entrance channel. These results suggest a new reaction mechanism for the oxidation of ethene by VO_2^+.

The values of the spin densities are different at both PESs. CP1 and CP2 at the triplet spin state present large values at the vanadium center (1.76 and 1.40, respectively) and at the C_1 carbon atom center (0.32 and 0.70, respectively). In the singlet state, the atomic spin density is approximately zero for all atoms; therefore, a change of the spin pairing on the vanadyl and ethylene moieties is necessary in the singlet state to reach the triplet spin state.

We have found two additional crossing points, CP3 and CP4, that do not have mechanistic significance, because they describe the crossing from the triplet to the singlet PES. However, from these points onward (to the products), the triplet PES becomes the lowest lying PES, and hence the crossing to the singlet PES will not take place. For the sake of completeness, the obtention and structure of these two crossing points at the B3LYP/6-31G* level is briefly described. CP3 is found for a scaled IRC value of $s = -0.58$ starting from t-TS8/9. The CP3 structure is shown in Figure 5 and is more similar to t-TS8/9 than to t-9. Energetically, however, CP3 lies 27.2 kcal/mol above t-9, while t-TS8/9 is 88.5 kcal/mol above t-9, and therefore CP3 is closer to t-9. Finally, CP4 is found for an IRC value of $s = -0.54$ in the IRC from t-TS10/11. The structure, shown in Figure 5, is similar to t-11 and energetically closer to this minimum (1.8 kcal/mol above) than to t-TS10/11 (which stands 23.3 kcal/mol above).

We can trace two reaction channels that connect the most stable reactants, VO_2^+ ($^1A_1$) + C_2H_4 (^1A_g), with the most stable products, VO^+ ($^3\Sigma$) + CH_3CHO ($^1A'$), both including crossing points (Figure 6). An analysis of these figures shows that except the separated reactants and products, the highest energy stationary point of the first pathway (Figure 6a) is s-TS1/2, which is 15.9 kcal/mol (17.4 at the B3LYP/6-31G* level) below the separated reactants and 1.5 kcal/mol (6.2 at B3LYP/6-31G*) below the triplet state separated products. For the second

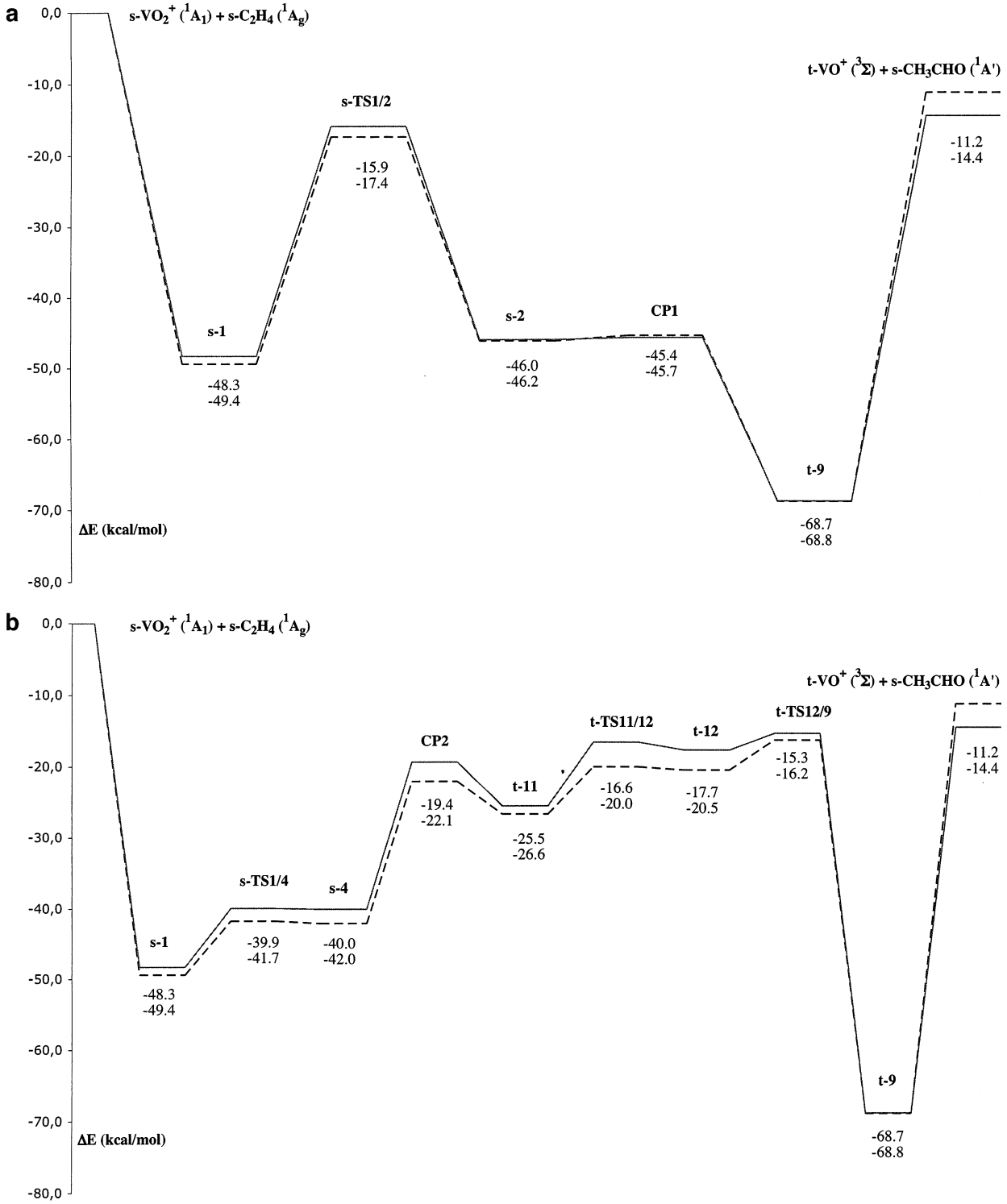

Figure 6. Overall energetics of the VO_2^+ ($^1A_1$) + C_2H_4 (^1A_g) → VO^+ ($^3\Sigma$) + CH_3CHO ($^1A'$) reaction based on ΔE values (kcal/mol) at the B3LYP/6-311G(2d,p) (solid line) and B3LYP/6-31G* (dashed line) levels. The total energy values of the singlet electronic state for the separated reactants are −1172.791 926 hartrees at the B3LYP/6-311G(2d,p) level and −1172.669 168 hartrees at the B3LYP/6-31G* level. (a) First pathway. (b) Second pathway.

pathway (Figure 6b), the highest energy stationary point is t-TS12/9, which is 15.3 kcal/mol (16.2 if using the small basis set) below the separated reactants and 0.9 kcal/mol (5 at B3LYP/6-31G*) below the separated products. The two pathways are found to have similar profiles: the difference of relative energy between the two highest energy stationary points is just 0.6 kcal/mol (1.2 at B3LYP/6-31G*). This difference is 0.8 kcal/mol if the Gibbs free energy values are compared (0.1 at B3LYP/6-31G*, see Figure 3a and d). This fact suggests that the two reaction mechanisms can be considered as competitive. A comparison with previous work by Schwarz et al.[49] shows that the present results provide a complete picture of the chemical rearrangement: the second competitive reaction path has been newly proposed and characterized, while the first reaction path has been completed with respect to the Schwarz proposal.

It must be noted that if Gibbs free energies at the B3LYP/6-311G(2d,p) level are taken into account, the highest energy point in what refers to the second pathway is t-TS11/12 instead

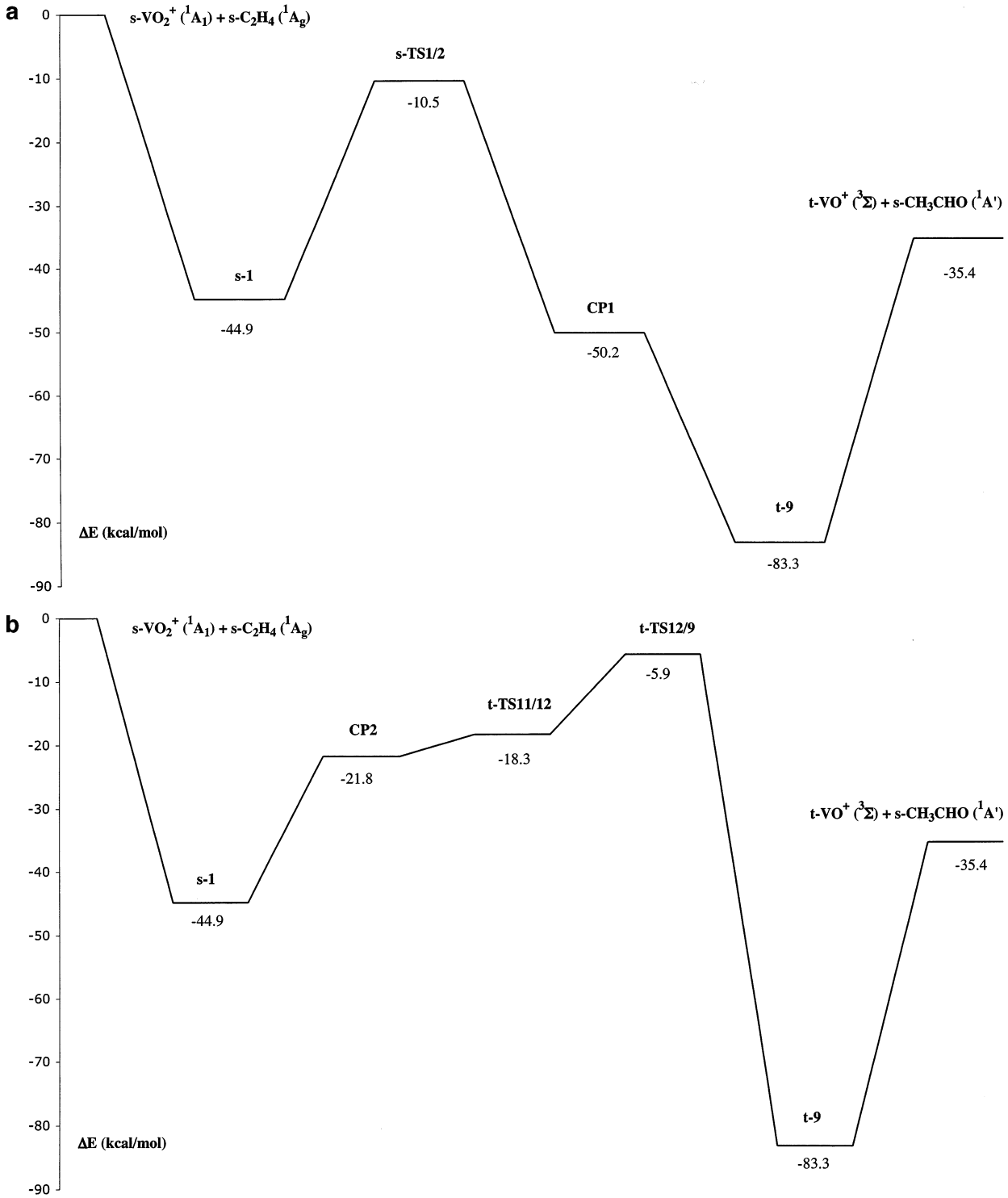

Figure 7. Relative energies (to the separated reactants) of some stationary points based on CCSD/6-311G(2d,p)//B3LYP/6-311G(2d,p) calculations. The total energy value of the singlet electronic state for the separated reactants is −1171.227 576 hartrees. (a) First pathway. (b) Second pathway.

of t-TS12/9, −6.0 kcal/mol and −6.1 kcal/mol, respectively. However, if Gibbs free energies at the B3LYP/6-31G* level or potential energies with the two basis sets are used, the highest energy point found for this pathway at the triplet state is t-TS12/9.

A final question can now be addressed: s-1 and t-9 are two common points for the two competing paths. They are the reactant and product complexes and are the most stable points. If talking about Gibbs free energy values (Figure 3), s-1 stands 35.9 kcal/mol, and t-9 57.5 kcal/mol, below separated reactants. From the reactants to products complexes, the process is therefore exothermic by 21.6 kcal/mol (20.6 kcal/mol at the B3LYP/6-31G* level). This trend is in agreement with the experimental data for the reaction of other vanadium cation clusters with ethylene derivatives.[48]

Single-point CCSD/6-311G(2d,p)//B3LYP/6-311G(2d,p) calculations have finally been carried out on the most relavant points of the reaction channels. Thus, the reactant and product complexes (s-1 and t-9), the crossing points (CP1 and CP2), and the highest energy stationary points (s-TS1/2 for the first pathway, and t-TS12/9 and t-TS11/12 for the second pathway) and separated products ($t\text{-}VO^+ + s\text{-}CH_3CHO$) have been

recalculated, with respect to the reference singlet state reactants, which have also been computed. The energetic values obtained are schematically depicted in Figure 7. An analysis of the results shows that the tendencies are maintained: a slight difference between the highest energy points (4.6 kcal/mol) favoring s-TS1/2 against t-TS12/9 is sensed, t-TS11/12 is found to be more stable than t-TS12/9 (by 12.4 kcal/mol), and the exothermic nature of the process from reactant to product complexes is increased to 38.4 kcal/mol, as compared with the ΔE values of 20.4 and 19.4 kcal/mol obtained at the B3LYP/6-311G (2d,p) and B3LYP/6-31G* levels, respectively.

4. Conclusions

A detailed study on the oxidation of C_2H_4 ($^1A_g/^3A_1$) by VO_2^+ ($^1A_1/^3A''$) to yield VO^+ ($^1\Delta/^3\Sigma$) and CH_3CHO ($^1A'/^3A''$) is reported. The singlet and lowest triplet states have been mapped out, and the regions where they cross were examined. We have characterized intermediates and TSs of the reaction pathways in both singlet and triplet electronic states using a hybrid density functional approach, B3LYP/6-31G* and B3LYP/6-311G(2d,p) levels. CCSD/6-311G(2d,p)//B3LYP/6-311G(2d,p) single-point calculations have also been carried out at relevant stationary points along the most favorable reaction pathways. The chemical reactivity patterns have been rationalized by geometrical and natural charge analysis of the stationary points and the CPs between both spin states. The conclusions of the present study can be summarized as follows:

(i) Two basis sets have been used, and a comparison has been made throughout the text between the results obtained in each case. In what refers to geometries, fluctuation patterns, and energetic profiles, the two approaches render very similar values. However, in what refers to charge distribution, the use of the large basis set is preferred.

(ii) Two competitive reaction pathways, including the crossing points CP1 and CP2, are found from the most stable reactants, VO_2^+ ($^1A_1$) + C_2H_4 (^1A_g), to the most thermodynamically stable products, VO^+ ($^3\Sigma$) + CH_3CHO ($^1A'$). The difference between the value of the relative energy of the highest transition structures that must be overcome for both pathways is low, around 0.6 kcal/mol (potential energy) or around 0.8 kcal/mol (Gibbs free energy).

(iii) The reactant and product complexes in the singlet and triplet electronic states, respectively, are the most stable points on the calculated paths. From the reactants to products complexes, the process is exothermic. Four CPs between both states have been found. Two of them have mechanistic significance. CP1 is found after s-2 and opens a direct pathway to t-9, the product complex. CP2 is found after s-4, and this spin crossing opens a lower barrier pathway to yield t-11. CP1 is not kinetically relevant because the rate-limiting step (the passage over s-TS1/2) is located in a previous stage, and the spin inversion is not regarded as a rate-limiting factor but rather as a later step occurring in the exit channel. However, CP2 is found before the rate-limiting step (most probably, the passage over t-TS12/9) is reached, and hence it takes place in the entrance channel, without the need to overcome the large barrier on the singlet PES.

Our present calculations are oversimplified in several aspects. We did not calculate spin−orbit coupling between electronic states of different multiplicities to estimate the crossing probabilities, and the effect of the quantum dynamics has not been taken into account. More quantitative calculations using more sophisticated computing methods are needed to answer many remaining questions. Nevertheless, to the best of our knowledge, this work is the first study of its kind to provide a detailed characterization of the chemical reactivity patterns of the VO_2^+ + C_2H_4 reaction in the singlet and triplet electronic states. The present study can be considered a clear-cut case of spin crossing effects to be important in determining the outcome of the chemical reaction. The information gained may provide a useful insight into the interaction of vanadyl cation and ethylene and improve the understanding of their chemical reactivity and suggest that spin effects may operate more generally on the kinetics of other related systems. Work is in progress to perform analogous studies for the oxidation reaction between different hydrocarbons and other metal oxide cations. While a valid mechanistic hypothesis with the present density functional computations is presented, it still needs to be substantiated by further theoretical studies at higher computing level and experimental data. The present work can be regarded as a starting point for the future studies.

Acknowledgment. The authors would like to thank the reviewers for helpful comments and suggestions to improve the previous version of the manuscript. This work is supported by DGI (project BQU2000-1425-C03-02) as well as by Fundació Caixa Castelló-Bancaixa (projects P1A99-2 and P1A99-16) and Brazilian Funding Agencies FAPESP (project 1999/03097-6) and CAPES. L.G. and M.C. are grateful to the Ministerio de Ciencia y Tecnología and Conselleria de Cultura, Educació i Ciència (Generalitat Valenciana), respectively, for doctoral fellowships. M.C. also acknowledges Universitat Jaume I for a postdoctoral fellowship. J.R.S. was visiting professor at Universitat Jaume I and acknowledges Fundació Caixa Castelló-Bancaixa and FAPESP for financial support. The computer facilities of the Servei d'Informàtica (Universitat Jaume I) and Laboratório de Simulaçao Molecular (Unesp, Bauru) are also acknowledged.

References and Notes

(1) Henrich, V. E.; Cox, P. A. *The surface science of metal oxides*; Cambridge University Press: Cambridge, 1994.
(2) *Metal-oxo and metal-peroxo species in catalytic oxidations*; Meunier, B., Ed.; Springer: Berlin, 2000.
(3) *The chemical dynamics and kinetics of small radicals. Parts I and II*; Liu, K., Wagner, A., Ed.; World Scientific: Singapore, 1995.
(4) Eller, K.; Schwarz, H. *Chem. Rev.* **1991**, *91*, 1121.
(5) Somorjai, G. A. *Introduction to surface chemistry and catalysis*; John Wiley & Sons: New York, 1994.
(6) Ponec, V. *J. Mol. Catal. A* **1998**, *133*, 221.
(7) Butler, L. J. *Annu. Rev. Phys. Chem.* **1998**, *49*, 125.
(8) Thoss, M.; Miller, W. H.; Stock, G. *J. Chem. Phys.* **2000**, *112*, 10282.
(9) Sugny, D.; Joyeux, M. *Chem. Phys. Lett.* **2001**, *337*, 319.
(10) Joyeux, M.; Sugny, D.; Lombardi, M. *Chem. Phys. Lett.* **2002**, *352*, 99.
(11) Nakamura, H. In *Dynamics of Molecules and Chemical Reactions*; Wyatt, R. E., Zhang, J. Z. H., Eds.; Dekker: New York, 1996.
(12) Bernardi, F.; Olivucci, M.; Robb, M. A. *Chem. Soc. Rev.* **1996**, *25*, 321.
(13) Yarkony, D. R. *Rev. Mod. Phys.* **1996**, *68*, 985.
(14) Yarkony, D. R. *J. Phys. Chem.* **1996**, *100*, 18612.
(15) Yarkony, D. R. *Acc. Chem. Res.* **1998**, *31*, 511.
(16) Zhu, C.; Nakamura, H.; Nobusada, K. *Phys. Chem. Chem. Phys.* **2000**, *2*, 557.
(17) Yarkony, D. R. *J. Phys. Chem. A* **2001**, *105*, 2642.
(18) Yarkony, D. R. *J. Phys. Chem. A* **2001**, *105*, 6277.
(19) Armentrout, P. B. *Science* **1991**, *251*, 175.
(20) Plattner, D. *Angew. Chem., Int. Ed. Engl.* **1999**, *38*, 82.
(21) Schröder, D.; Shaik, S.; Schwarz, H. *Acc. Chem. Res.* **2000**, *33*, 139.
(22) Schröder, D.; Schwarz, H.; Shaik, S. In *Metal-Oxo and Metal-Peroxo Species in Catalytic Oxidations*; Meunier, B., Ed.; Springer-Verlag: Berlin, 2000; pp 91−123.
(23) Zhang, J.; Riehn, C. W.; Wittig, C. *J. Chem. Phys.* **1995**, *103*, 6815.
(24) Cui, Q.; Morokuma, K. *Chem. Phys. Lett.* **1997**, *272*, 319.

(25) Irigoras, A.; Fowler, J. E.; Ugalde, J. M. *J. Am. Chem. Soc.* **1999**, *121*, 574.
(26) Irigoras, A.; Fowler, J. E.; Ugalde, J. M. *J. Am. Chem. Soc.* **1999**, *121*, 8549.
(27) Irigoras, A. Doctoral Ph.D. Thesis, Universidad del País Vasco, 1999.
(28) Bearpark, M. J.; Deumal, M.; Robb, M. A.; Vreven, T.; Yamamoto, N.; Olivucci, M.; Bernardi, F. *J. Am. Chem. Soc.* **1997**, *119*, 709.
(29) Yoshizawa, K.; Shiota, Y.; Yamabe, T. *J. Chem. Phys.* **1999**, *111*, 538.
(30) Yoshizawa, K.; Shiota, Y.; Yamabe, T. *J. Am. Chem. Soc.* **1999**, *121*, 147.
(31) Wilsey, S.; Bernardi, F.; Olivucci, M.; Robb, M. A.; Murphy, S.; Adam, W. *J. Phys. Chem. A* **1999**, *103*, 1669.
(32) Danovich, D.; Shaik, S. *J. Am. Chem. Soc.* **1997**, *119*, 1773.
(33) Filatov, M.; Shaik, S. *J. Phys. Chem. A* **1998**, *102*, 3835.
(34) Rue, C.; Armentrout, P. B.; Schwarz, H. *J. Chem. Phys.* **1999**, *110*, 7858.
(35) Poli, R. *Chem. Rev.* **1996**, *96*, 2135.
(36) Keogh, D. W.; Poli, R. *J. Am. Chem. Soc.* **1997**, *119*, 2516.
(37) Linde, C.; Akermark, B.; Norrby, P.-O.; Svensson, M. *J. Am. Chem. Soc.* **1999**, *121*, 5083.
(38) Gorelsky, S. I.; Lavrov, V. V.; Koyanagi, G. K.; Hopkinson, A. C.; Bohme, D. K. *J. Phys. Chem. A* **2001**, *105*, 9410.
(39) El-Bahraoui, J.; Wiest, O.; Feichtinger, D.; Plattner, D. A. *Angew. Chem., Int. Ed.* **2001**, *40*, 2073.
(40) Hess, J. S.; Leelasubcharoen, S.; Rheingold, A. L.; Doren, D. J.; Theopold, K. H. *J. Am. Chem. Soc.* **2002**, *124*, 2454.
(41) Shaik, S.; Danovich, D.; Fiedler, A.; Schröder, D.; Schwarz, H. *Helv. Chim. Acta* **1995**, *78*, 1393.
(42) Bell, R. C.; Zemski, K. A.; Kerns, K. P.; Deng, H. T.; Castleman, A. W., Jr. *J. Phys. Chem. A* **1998**, *102*, 1733.
(43) Bell, R. C.; Zemski, K. A.; Castleman, A. W., Jr. *J. Phys. Chem. A* **1998**, *102*, 8293.
(44) Bell, R. C.; Zemski, K. A.; Castleman, A. W., Jr. *J. Phys. Chem. A* **1999**, *103*, 1585.
(45) Bell, R. C.; Zemski, K. A.; Castleman, A. W., Jr. *J. Phys. Chem. A* **1999**, *103*, 2992.
(46) Kooi, S. E.; Castleman, A. W., Jr. *J. Phys. Chem. A* **1999**, *103*, 5671.
(47) Bell, R. C.; Zemski, K. A.; Justes, D. R.; Castleman, A. W., Jr. *J. Chem. Phys.* **2001**, *114*, 798.
(48) Zemski, K. A.; Justes, D. R.; Castleman, A. W., Jr. *J. Phys. Chem. A* **2001**, *105*, 10237.
(49) Harvey, J. N.; Diefenbach, M.; Schröder, D.; Schwarz, H. *Int. J. Mass Spectrom.* **1999**, *182/183*, 85.
(50) Frisch, M. J.; Trucks, G. W.; Schlegel, H. B.; Scuseria, G. E.; Robb, M. A.; Cheeseman, J. R.; Zakrzewski, V. G.; Montgomery, J. A.; Stratmann, R. E.; Burant, J. C.; Dapprich, S.; Millam, J. M.; Daniels, A. D.; Kudin, K. N.; Strain, M. C.; Farkas, O.; Tomasi, J.; Barone, V.; Cossi, M.; Cammi, R.; Mennucci, B.; Pomelli, C.; Adamo, C.; Clifford, S.; Ochterski, J.; Petersson, G. A.; Ayala, P. Y.; Cui, Q.; Morokuma, K.; Malick, D. K.; Rabuck, A. D.; Raghavachari, K.; Foresman, J. B.; Cioslowski, J.; Ortiz, J. V.; Stefanov, B. B.; Liu, G.; Liashenko, A.; Piskorz, P.; Komaromi, I.; Gomperts, R.; Martin, R. L.; Fox, D. J.; Keith, T.; Al-Laham, M. A.; Peng, C. Y.; Nanayakkara, A.; Gonzalez, C.; Challacombe, M.; Gill, P. M. W.; Johnson, B. G.; Chen, W.; Wong, M. W.; Andres, J. L.; Head-Gordon, M.; Replogle, E. S.; Pople, J. A. *Gaussian98 (Revision A.1)*; Gaussian, Inc.: Pittsburgh, PA, 1998.
(51) Lee, C.; Yang, R. G.; Parr, R. G. *Phys. Rev. B* **1988**, *37*, 785.
(52) Becke, A. D. *J. Chem. Phys.* **1993**, *98*, 5648.
(53) Rassolov, V. A.; Pople, J. A.; Windus, T. L. *J. Chem. Phys.* **1998**, *109*, 1223.
(54) Calatayud, M.; Andrés, J.; Beltrán, A. *J. Phys. Chem. A* **2001**, *105*, 9760.
(55) Calatayud, M.; Andrés, J.; Beltrán, A.; Silvi, B. *Theor. Chem. Acc.* **2001**, *105*, 299.
(56) Calatayud, M.; Silvi, B.; Andrés, J.; Beltrán, A. *Chem. Phys. Lett.* **2001**, *333*, 493.
(57) Pople, J. A.; Head-Gordon, M.; Raghavachari, K. *J. Chem. Phys.* **1987**, *87*, 5968.
(58) McIver, J. W., Jr. *Acc. Chem. Res.* **1974**, *7*, 72.
(59) Fukui, K. *J. Phys. Chem.* **1970**, *74*, 4161.
(60) González, C.; Schlegel, H. B. *J. Chem. Phys.* **1989**, *90*, 2154.
(61) González, C.; Schlegel, H. B. *J. Phys. Chem.* **1990**, *94*, 5523.
(62) Poli, R.; Harvey, J. N. *Chem. Soc. Rev.* **2003**, *32*, 1.
(63) Reed, A. E.; Weinstock, R. B.; Weinhold, F. *J. Chem. Phys.* **1985**, *83*, 735.
(64) Reed, A. E.; Curtiss, L. A.; Weinhold, F. *Chem. Rev.* **1988**, *88*, 899.